SPATIAL AUDIO AND REVERBERATION MODELING USING HYPERDIMENSIONAL DIGITAL WAVEGUIDE MESHES

Antti Kelloniemi[1)], *Patty Huang*[2,3)], *Vesa Välimäki*[3)], *and Lauri Savioja*[1)]

[1)] Telecommunications Software and Multimedia Laboratory, Helsinki University of Technology
P.O. Box 5400, FI-02015 TKK, Finland
phone: +358 9 4511, fax: +358 9 451 5014, emails: antti.kelloniemi@panphonics.fi, lauri.savioja@tkk.fi

[2)]CCRMA, Department of Music, Stanford University
Stanford, CA 94305-8180, USA
email: pph@ccrma.stanford.edu

[3)]Laboratory of Acoustics and Audio Signal Processing, Helsinki University of Technology
P.O. Box 3000, FI-02015 TKK, Finland
email: vesa.valimaki@tkk.fi

ABSTRACT

Characteristics of digital waveguide meshes with more than three physical dimensions are studied. Especially, the properties of a 4-D mesh are analyzed and compared to waveguide structures of lower dimensionalities. The hypermesh produces a response with a dense and irregular modal pattern at high frequencies, which is beneficial in modeling the reverberation of rooms or musical instrument bodies. In addition, it offers a high degree of decorrelation between output points selected at different locations, which is advantageous for multi-channel reverberation. The frequency-dependent decay of the hypermesh response can be controlled using boundary filters introduced recently by one of the authors. Several hypermeshes can be effectively combined in a multirate system, in which each mesh produces reverberation on a finite frequency band. The paper presents three hypermesh application examples: a multi-channel reverberation algorithm, the modeling of the impulse response of a lecture hall, and the simulation of the response of a clavichord soundbox.
Keywords: acoustic signal processing, architectural acoustics, FDTD methods, acoustic propagation, multidimensional systems, music

1. INTRODUCTION

The hyperdimensional digital waveguide (DWG) mesh is a 4-D version of the algorithm introduced by Van Duyne and Smith [1, 2]. There have been plenty of applications of the DWG mesh technique, but they have been limited to maximally three dimensions. 1-D digital waveguides are mostly used for simulating wave propagation in strings and tubes [3, 4, 5], 2-D meshes are applied in plate or membrane simulations [6, 7, 8, 9, 10], while rooms and resonant bodies of musical instruments are modeled with 3-D meshes [11, 12, 13, 9, 14, 15, 16]. Researchers have also modeled resonant objects and spaces with meshes having the number of dimensions different from that of the modeled object. For example, 2-D DWG meshes have been employed in room acoustic modeling [17, 18]. Recently, Mullen et al. have shown that a 2-D waveguide is an effective tool for simulating narrow acoustic tubes, which essentially contain a 1-D acoustic field [19].

The idea of the hyperdimensional mesh was mentioned already in the original 2-D DWG mesh paper by Van Duyne and Smith [1], and later suggested again, for example, by Savioja et al. [11] and Rocchesso and Smith [20]. In this paper, we investigate the properties of the 4-D mesh and possibilites opened by it through practical examples. Special emphasis is on employing the technique on reverberation modeling.

Artificial reverberation is widely used in musical performances and recordings. In addition to its use as an effect or in room acoustic simulation, reverberation modeling is needed in the synthesis of musical instruments with a resonating body, such as the soundbox or soundboard of stringed keyboard instruments.

This paper is organized as follows. Section 2 discusses the normal modes of vibration in enclosed spaces. In Section 3, the hyperdimensional DWG mesh, or the hypermesh for short, is discussed as an extension to the previously known waveguide mesh methods. Section 4 describes the application of the hypermesh in three different cases of artificial reverberation: multi-channel reverberation, simulation of a lecture hall's impulse response, and simulation of the soundbox of a musical keyboard instrument.

2. NORMAL MODES IN ENCLOSURES WITH RIGID BOUNDARIES

Sound pressure waves reflect from boundaries, such as walls and furniture in a room. When the time interval between successively received reflected sounds is short, they are perceived as reverberation instead of individual echoes. In any closed space, sound is reflected along multiple closed propagation paths, and thus standing waves occur. The standing waves determine the modal structure in the frequency response of the acoustic system. At low frequencies, the modes are sparsely spaced in frequency, but at frequencies above a critical frequency, often called the Schroeder frequency, the sound field is diffuse and modes are not distinguished individually by the ear [21, 22]. If the modal density created by an artificial reverberation algorithm is too low in this high frequency region, tonality or a metallic timbre is perceived.

This work was funded by the Academy of Finland (project no. 201050) and the Nokia Foundation. The authors would like to extend their thanks to Dr. Tapio Lokki for the room impulse response measurement data, to Dr. Cumhur Erkut and Dr. Mikael Laurson for the clavichord recordings, and to Mr. Seppo Paulin for Fig. 4.

Sound pressure between two rigid boundaries located at $x = 0$ and $x = L$ must fulfill the boundary condition

$$\frac{dp}{dx} = 0. \tag{1}$$

The sound pressure value at a certain modal frequency at any point is given by a solution for (1) that can be written as

$$p(x) = A\cos(k_n x), \tag{2}$$

where A is an arbitrary coefficient, $k_n = n\pi/L$, and $n = 0, 1, 2, \ldots$ is the integer index of the current mode along dimension x having corresponding length L [22].

The 1-D solution can be extended to N dimensions, where the sound pressure value at point $(x_1, x_2, \ldots, x_N)$ inside the N-dimensional rectangular space at a certain modal frequency is

$$p_{n_1 n_2 \ldots n_N}(x_1, x_2, \ldots, x_N) = B\prod_{i=1}^{N}\cos(k_{n_i} x_i), \tag{3}$$

where B is an arbitrary coefficient. The modes appear at frequencies

$$f_{n_1 n_2 \ldots n_N} = \frac{c}{2\pi} k_{n_1 n_2 \ldots n_N}, \tag{4}$$

where c is the sound velocity. The constant $k_{n_1 n_2 \ldots n_N}$ is a combination of all k_{n_i}:

$$k_{n_1 n_2 \ldots n_N} = \pi\left[\sum_{i=1}^{N}\left(\frac{n_i}{L_i}\right)^2\right]^{1/2}. \tag{5}$$

The first axial standing wave along each dimension with $n_i = 1$ has a frequency whose corresponding wavelength is equal to twice the trajectory length. Other standing waves on the same trajectory are created at multiples of this base frequency. In addition to these 1-D modes occurring between perpendicular boundaries, multidimensional standing waves are supported as closed propagation paths are created between multiple boundaries. For these diagonal and oblique modes, two or more indices have values above zero, respectively.

The modal frequencies are inversely proportional to the trajectory length, so, for example in large halls the modes start from lower frequencies than in small rooms. The modal density also increases with frequency, as suggested by (4) and (5). Actual rooms and halls are not perfectly rectangular and have furniture and other objects affecting sound propagation. So the trajectory lengths are not equal at all frequencies. More propagation trajectories are supported, especially at high frequencies, resulting in an even denser and inharmonic modal structure. In more complex shapes, such as fan-shaped rooms or bodies of musical instruments, the modal structure is too complex to be managed in closed form expressions. Instead, numerical approximations of the wave propagation are needed.

3. DIGITAL WAVEGUIDE MESH METHOD

The DWG mesh provides a computational model for multidimensional wave propagation. It was created as an extension of 1-D digital waveguides popular in the physical modeling-based sound synthesis applications [1, 23]. A 1-D DWG consists of two delay lines passing signals into opposite directions and scattering junctions between the delay lines. The input signal to a junction can be passed through, partially transmitted, or reflected back.

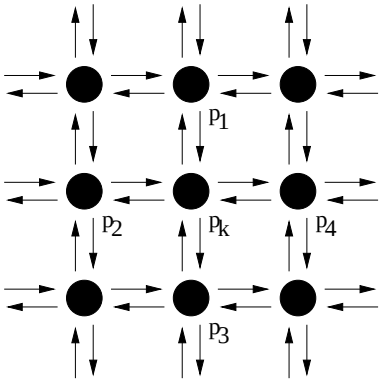

Figure 1: A two-dimensional rectilinear DWG mesh structure. p_k is the junction currently calculated and p_l, where $l = 1, 2, 3$, or 4, are its axial neighbors as in (8).

The mesh can be constructed in various ways. The choice can be made between two different variable types and multiple topologies. Common to all DWG mesh schemes is the regular discretization, both in time and in space.

3.1 The digital waveguide mesh updating functions

A DWG mesh consists of bidirectional delay lines and scattering junctions connecting them at regular nodal points. For example, a 2-D DWG mesh structure is shown in Fig. 1. In a homogeneous N-dimensional mesh each junction has $2N$ neighbors, and all interconnections have equal impedances. If the delays are located at the interconnections of the nodes, the updating function of each junction is written as

$$p_k(n) = \frac{2}{N}\sum_l p_l^+(n), \tag{6}$$

where $p_l^+(n)$ are the incoming wave variable values of each interconnection l of the current junction at time instant n. The outgoing values are then updated using the current junction value p_k:

$$p_l^-(n) = p_k(n) - p_l^+(n). \tag{7}$$

The outgoing values are transformed into ingoing values of neighboring junctions when they are passed by the unit delays in the interconnections during the next computational time step. This formulation of the mesh is called the wave variable formulation, or W mesh.

Another formulation of the same functionality uses physically measurable variables instead of their traveling wave decomposition, as used in (6) and (7). In the so-called Kirchhoff formulation, or K mesh, the delays are located at the nodal points of the mesh, and the updating function of each junction is written as

$$p_k(n) = \frac{\sum_l p_l(n-1)}{N} - p_k(n-2), \tag{8}$$

where p_l are now the values of the neighboring junctions. While being numerically less robust, in multi-dimensional models this formulation requires considerably less main system memory than an equivalent W mesh [24].

The sampling frequency is related to the dimensionality N of the mesh by

$$f_s = \frac{c\sqrt{N}}{\Delta x}, \tag{9}$$

where c is the wave propagation speed in the mesh and Δx is the spatial sampling interval corresponding to the distance between two neighboring junctions [13]. The practical frequency bandwidth for the mesh depends on its geometric topology [25]. For example, a triangular mesh cannot produce resonances above $f_s/3$ and a rectilinear mesh has a spectrum that mirrors itself at $f_s/4$. Due to the mirroring of resonances around half the Nyquist limit, the output of a rectilinear mesh is usually lowpass filtered in order to retain only the "unique" modes below $f_s/4$. However, this filtering is not required if the user is only interested in having an output with a maximal number of modes instead of an exact physical model of a resonating structure.

In a DWG mesh, the number of degrees of freedom of the model is equal to the number of delay elements. So in a homogeneous and freely resonating rectilinear K mesh the maximum number of modes below the mirroring frequency is equal to the number of junctions. The highest mode index number n_i is equal to the number of junctions along the corresponding dimension. If the phase of the reflected wave is preserved at the boundary, $n_i \geq 0$. In the case of phase reversing reflection, the lowest modes are canceled, and only modes with $n_i \geq 1$ are supported.

3.2 Hyperdimensional DWG mesh structure

The mesh dimensionality N is not restricted to the limits of our physical world. Instead, hyperdimensional meshes are easy to construct by adding more interconnections between the scattering junctions [20, 13, 26].

As seen in Fig. 2, the modes are distributed equally in a 1-D DWG structure. In rectilinear meshes with higher dimensionalities, the modes are densest near $f_s/4$ and sparsest at frequencies close to DC and $f_s/2$. As the number of junctions is kept constant with increasing dimensionality, the number of junctions along each dimension is diminished. This packs the modes closer around $f_s/4$. At the same time, the modal frequencies become higher because the sampling frequency increases with dimensionality, as seen from (9). The number of independent indices n_i in (5) is equal to the number of dimensions. Maximizing the number of dimensions and choosing the L_i values close together from a prime number series minimizes the harmonicity of the mode distribution, which is beneficial for simulating reverberation over a wide frequency bandwidth [27]. The inharmonicity is further augmented by perturbation in mode frequencies caused by the numerical dispersion inherent in the waveguide mesh structure [2, 8].

3.3 Boundary conditions

For realistic reverberation modeling, frequency-dependent losses have to be implemented. In real rooms, high frequencies usually decay faster than low frequencies due to absorption of energy by air and wall materials. Another important feature is the strong modal frequencies with long decay times

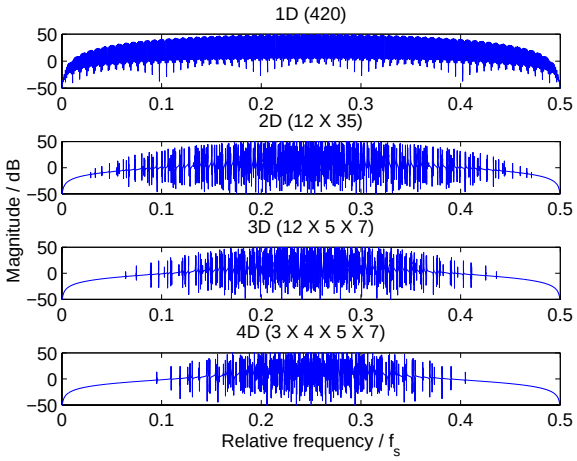

Figure 2: Frequency responses of rectilinear meshes with 420 scattering junctions, organized in four different dimensionalities. The reflection coefficient of all boundaries was $R = -1$. The mesh was initialized at a corner junction, and the output was read at the same location.

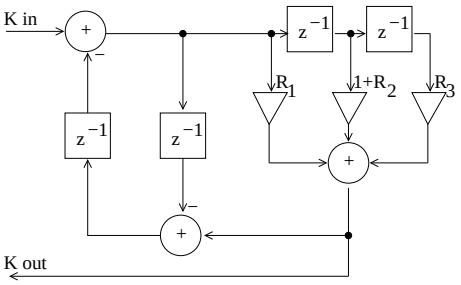

Figure 3: The boundary junction with KW-conversion and second-order FIR filter [28].

characterizing some spaces, especially musical instrument bodies.

In a DWG mesh, the frequency-dependent losses can be combined and implemented with boundary filters. In this way the inner mesh structure is kept lossless and homogeneous. As discussed earlier, the inner mesh was implemented using K formulation. As boundary filters are easier to design for traveling wave variables, a boundary junction structure including a variable-type converter and a second-order FIR filter was used, as depicted in Fig. 3 [28].

The boundary reflection characteristics are determined with coefficients R_1, R_2, and R_3. This kind of low-order filter can model simple lowpass behavior and is effective enough for nonexact simulation of impulse responses.

4. APPLICATION TO ARTIFICIAL REVERBERATION

The frequency response of a reverberant structure can be coarsely divided into two bands. At low frequencies, the modes can be individually heard. Their frequencies and decay times are psychoacoustically important, so recreating them exactly is needed for convincingly simulating the response. At higher frequencies, the modal frequencies are not heard individually, and thus an exact physical model is not

needed. For natural sounding simulation of high-frequency reverberation, the key issues are the density and the irregularity of the modal structure [27].

In the first of the three examples presented here, the hypermesh structure is used for creating multi-channel reverberation. In the following two examples, it is used to generate the high-frequency portion of the impulse responses of a lecture hall and a clavichord soundbox. In both cases, the high-frequency hypermesh response is combined with the output of other resonator models providing the low-frequency modes at physically correct frequencies. This is similar to hybrid models which have been used for simulating bodies of musical instruments, in which a reverberation algorithm is combined with a resonator bank in parallel [14, 29].

Sound samples of the studied cases are available at http://www.acoustics.hut.fi/∼vpv/publications/hypermesh/.

4.1 Case: Multi-channel reverb

The growth of multi-channel audio formats has generated a demand for multi-channel sound effects and reverberators. These may be used for adding spaciousness to a movie soundtrack, for example, but they are also needed in electroacoustic systems designed for the control of reverberation in multipurpose halls, or when the acoustics of a concert hall are modified with an active system installation.

In all these cases, the spatial impression is achieved by producing diffuse-sounding reverberation. It has been shown that to attain a subjectively good spacious reverberant sound, the synthetic reflections must be derived from the same original signal and, most importantly, demonstrate mutual incoherence [22]. The degree of coherence can be expressed by the correlation coefficient

$$S(s_1, s_2) = \frac{C(s_1, s_2)}{\sqrt{C(s_1, s_1)C(s_2, s_2)}}, \qquad (10)$$

where s_1 and s_2 are samples of two signals and C is the covariance value between the two samples.

DWG mesh algorithms have the benefit of providing multiple outputs for one input at the same computational cost. Thus, to implement a multi-channel reverberation algorithm, only the values of several junctions have to be recorded at each time step, contrary to computing the impulse responses separately for each channel.

For comparison, two 3-D meshes and a 4-D mesh were initialized at a corner (the junction with the lowest indices in all dimensions), and the responses were recorded for 10000 timesteps at four other corners. The meshes were set to be lossless. The first of the 3-D meshes was chosen to have an equal number of junctions with the 4-D mesh. The second 3-D mesh has a computational cost equal to that of the 4-D mesh, if summations and multiplications are regarded as equally expensive.

The resulting correlation coefficients between the responses and the probability values for testing the hypothesis of no correlation are listed in Table 1. The correlation is weaker between the two signals obtained at different points from the 4-D mesh than from the 3-D mesh in all but one of the example cases. The values of P denote the probability of getting a correlation as large as the observed value by random chance if $S = 0$. If the probability is small, $P < 0.05$, correlation is significant. The results in Table 1 indicate that there is no significant correlation in the case of the 4-D mesh,

Table 1: Correlation coefficients S between the received signals at two points and probability values P for the hypothesis of no correlation for the received responses in two 3-D meshes having (a) $7 \times 11 \times 15$ and (b) $9 \times 11 \times 15$ junctions, and in a 4-D mesh of $3 \times 5 \times 7 \times 11$ junctions. $S = 1$ means perfectly similar signals, values of $P < 0.05$ denote significant correlation. The P values greater than 0.05 are highlighted.

Mesh	Receiver 1	Receiver 2	S	P
3-D	(7,11,15)	(7,1,1)	0.0204	0.0410
(a)	(7,11,15)	(1,11,1)	0.0449	0.0000
	(7,11,15)	(1,1,15)	-0.0350	0.0005
	(7,1,1)	(1,11,1)	-0.0333	0.0009
	(7,1,1)	(1,1,15)	0.0464	0.0000
	(1,11,1)	(1,1,15)	-0.0254	0.0110
3-D	(9,11,15)	(9,1,1)	-0.0183	**0.0672**
(b)	(9,11,15)	(1,11,1)	-0.0187	**0.0622**
	(9,11,15)	(1,1,15)	0.1088	0.0000
	(9,1,1)	(1,11,1)	0.0936	0.0000
	(9,1,1)	(1,1,15)	0.0299	0.0028
	(1,11,1)	(1,1,15)	-0.0006	**0.9522**
4-D	(3,5,7,11)	(3,1,1,1)	0.0159	**0.1126**
	(3,5,7,11)	(1,5,1,1)	-0.0077	**0.4416**
	(3,5,7,11)	(1,1,7,1)	-0.0019	**0.8456**
	(3,1,1,1)	(1,5,1,1)	0.0149	**0.1367**
	(3,1,1,1)	(1,1,7,1)	0.0013	**0.8979**
	(1,5,1,1)	(1,1,7,1)	-0.0008	**0.9328**

whereas most of the 3-D mesh output pairs correlate significantly.

4.2 Case: Lecture hall

In the second example, the hypermesh is applied to the simulation of room reverberation. The impulse response of lecture hall T3 at the Helsinki University of Technology was measured and used as a reference. The dimensions of the lecture hall are shown in Fig. 4. The ceiling area is smaller than the floor area, as the left-side wall and the back wall are sloping. A soft absorbent plate is hung at 0.40 m below the ceiling, covering the full area from the back wall to 3.0 m from the front wall.

The room impulse response was measured 5.5 m from the left wall and 10.0 m from the front wall at a height of 1.7 m. The speaker used as a sound source was located 2.7 m away from both the left and the front wall equally, at a height of 1.2 m. The five most prominent frequency modes and their corresponding 60 dB decay times are listed in Table 2. They were evaluated from the measured signal and then removed from it.

A two-pole, two-zero inverse filter was designed for mode removal after determining the frequencies and decay times. The T_{60}s were estimated by fitting a straight line to the time-domain values of the response's energy decay relief (EDR) [30] at the frequency bin associated with a particular mode. The slope of the line was then inverted and scaled to obtain the T_{60} value. The zeros of each inverse filter are complex conjugates whose angles are the positive and negative radian frequency of the mode to be removed and whose radius R is matched to the T_{60} of the same mode by the rela-

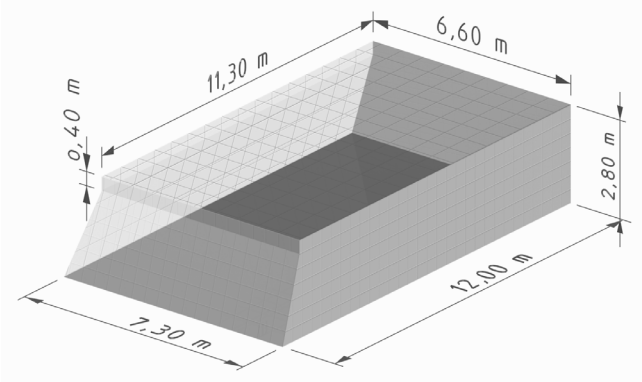

Figure 4: Dimensions of the lecture hall T3 at the Helsinki University of Technology.

Table 2: Analysis results for prominent modes of the lecture hall impulse response, to be implemented with a resonator bank.

Frequency (Hz)	T_{60} (sec)	Magnitude (dB)
75.96	0.8134	-25.90
102.52	1.3244	-30.58
122.02	1.4195	-29.31
138.08	0.9622	-31.85
148.02	1.3221	-29.02

tionship $R = e^{\frac{\ln(0.001)}{T_{60} f_s}}$. The two poles are identical to the zeros except that the radius is slightly contracted by a factor very close to 1, in order to isolate the effect of the zeros to the target mode [31]. 0.9999 was used when neighboring modes are very close to each other, but a factor of 0.999 was sufficient in most cases. The reverberation time of the remaining signal was evaluated on octave bands, and these T_{60} values were used as the optimization goal for the 4-D meshes.

The five highest octave bands with central frequencies from 1 kHz to 16 kHz were simulated by a multirate system consisting of two rectilinear 4-D meshes of $7 \times 8 \times 10 \times 13$ junctions each. The boundary filters shown in Fig. 3 were implemented at one end of the longest dimension, while perfectly reflecting, phase inversing conditions were implemented at other boundaries by fixing their values to zero. The simulation was run for 48000 time steps for the first mesh, and for 12000 steps for the second mesh, as its output was upsampled by a factor of 4. A Nyquist filter was used for anti-aliasing. The coefficients of the 3-tap FIR filters at one $7 \times 8 \times 10$ junction boundary of each mesh were optimized for minimizing the maximum error in T_{60}-values of the combined output. A Nelder-Mead optimization, provided by Matlab, was used.

At lower frequencies, the exact frequencies of each mode are perceptually important, and thus simulating only the decay times would not provide an appropriate result. Instead, a 3-D triangular mesh, also known as a 3-D dodecahedral or hexagonal close packed, was defined to model the low-frequency response. The low-frequency mesh topology was chosen by the fact that the dense triangular mesh exhibits minimal numerical errors. The mesh dimensions were designed to match the room dimensions as closely as possible

Table 3: Filter coefficients of the room impulse response simulation.

Boundary	R_1, R_3	R_2
3D hard walls	0.01958	0.84000
3D soft ceiling	0.00896	0.85918
4D mid frequencies	0.00440	0.67470
4D high frequencies	0.00200	0.91200

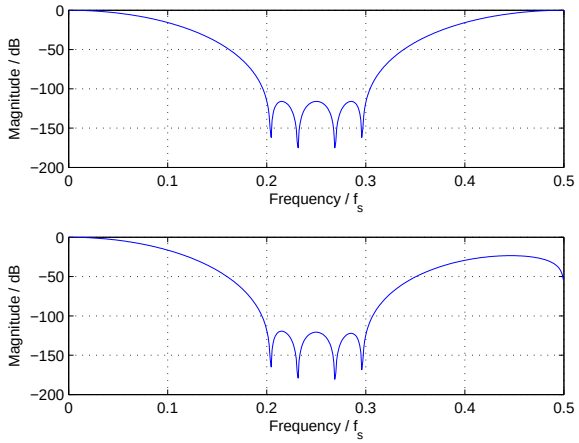

Figure 5: Frequency responses of the input filters of the two hypermeshes used in the room impulse response simulation: above for the mid frequencies and below for the highest frequencies.

with junction spacing of 0.2 m. Using (9), the sampling frequency of the mesh is seen to be $f_s \approx 2.9$ kHz and the highest frequency modeled is thus about 950 Hz. Linear-phase FIR filters were designed for all boundaries of the mesh. Two different sets of filter coefficients were optimized to match the reverberation times of the received signal to the measurement results. One filter was used for the soft ceiling, another for other surfaces. The coefficients used are listed in Table 3. The two hypermeshes were excited with impulse responses of high-order filters to match their frequency responses together at crossover frequencies. The frequency responses of the filters are shown in Fig. 5. The 3-D mesh was excited with a unit impulse. The measured and simulated T_{60} values are shown in Table 4, and the responses can be seen in Figs. 6 and 7, respectively. The resulting responses can be seen to be a good match in terms of reverberation times, especially at the frequencies above 1 kHz modeled specifically by the hypermeshes. The initial shapes of the frequency responses are significantly different, as the equalization of the relative magnitudes of the mesh outputs was set only by ear. This affects the first 0.1 seconds of the response. The difference in the latter part of the signals is explained by the noise present in the measured response in Fig. 6 and absent in the simulated response in Fig. 7. Also, the low-frequency model could have been implemented more precisely for a better match, but it was not the focus of this paper.

Table 4: Reverberation times of the measured and simulated room impulse responses of the lecture hall T3. Center-frequencies of the octave bands are listed.

Frequency (Hz)	Measured T_{60}	Simulated T_{60}
125	1.4640	0.5116
250	0.7403	0.6437
500	0.6503	0.4493
1000	0.5833	0.4277
2000	0.5640	0.5146
4000	0.5221	0.5212
8000	0.4739	0.4876
16000	0.3526	0.3388

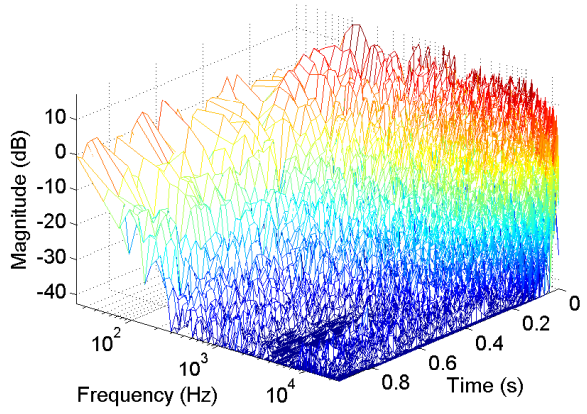

Figure 6: Measured impulse response of the lecture hall.

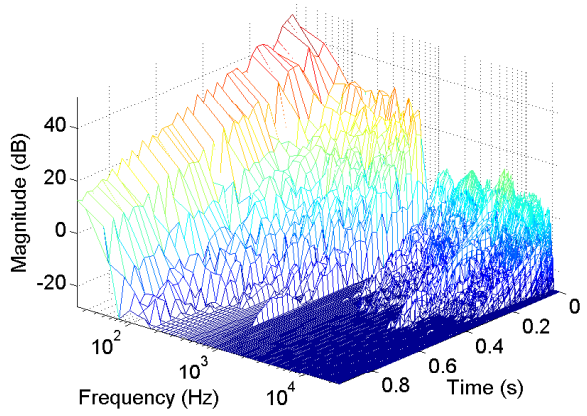

Figure 7: Simulated impulse response combined from the outputs of a 3-D triangular mesh for low frequencies and two 4-D hypermeshes for the frequencies above 700 Hz.

4.3 Case: Clavichord soundbox

In our last example, the reverberant impulse response of a clavichord soundbox was modeled using two hypermeshes and a resonator bank. The response used as the overall simulation target was produced with an impulse hammer impact on the soundbox while the strings of the clavichord were carefully damped. Figure 8 shows the time-frequency representation of the impulse response of the clavichord soundbox. It contains many modes between about 30 Hz and 3 kHz, but no significant energy at frequencies higher than that.

The hypermeshes served to generate an approximation of the dense high-frequency modes of the soundbox. The hypermesh simulation target was the soundbox impulse response whose long-ringing modes in the low-frequency range were removed by inverse filtering [31]. 28 biquadratic resonators were used to isolate the prominent modes below 500 Hz. Fewer resonators can be used in practice depending on the desired synthesis quality.

A multirate system was created, as in Section 4.2, to implement the soundbox reverberator in Fig. 9. Only two hypermeshes of $8 \times 9 \times 11 \times 13$ junctions were needed to generate sufficiently dense reverberation within the reduced bandwidth. The output of one of the meshes was upsampled by a factor of 3. The total response was filtered with a sixth-order LPC filter, whose coefficients were obtained from the measured soundbox impulse response after extracting the most prominent modes. Boundary filters were designed to match the decay times which were analyzed for each one third-octave band. The meshes were initialized with a filter output signal having a frequency response as depicted in Fig. 10.

Figure 11 is the time-frequency representation of the hypermesh model of the high-frequency response of the clavichord soundbox. The low-frequency modes that have been extracted are not included in this model. It is seen by comparing Figs. 8 and 11 that the hypermesh model produces a similar, but not exactly identical, response between about 100 Hz and 2 kHz. The low-frequency modes need to be implemented with separate resonators to obtain a full model of the soundbox.

The commuted synthesis [32, 33] clavichord model described in an article by V. Välimäki et al. [34] can be enhanced by replacing the sampled soundbox response triggered at each note with a soundbox reverberation module, such as the one described above. In a synthesis model using this scheme, the output of a string module would be fed into a body/resonator module as shown in Fig. 9. A similar solution has been used for sound synthesis of the harpsichord, where reverberation from the soundboard was simulated with a feedback delay network reverberator [35].

A reverberator model with a spatial interpretation such as the hypermesh supports multiple input locations and allows for subtle differences in reverberation for each note. This would be analogous to subtle differences in the soundbox response resulting from each string's unique driving point on the bridge. The contribution of a hypermesh reverberator to a synthetic clavichord tone makes it sound more realistic and lively than if it were only overlaid with a sampled soundbox impulse response, which always adds the same reverberation effect to the tone.

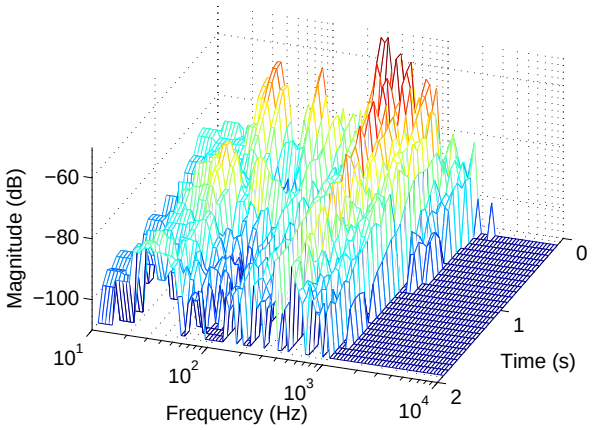

Figure 8: Measured impulse response of the clavichord soundbox.

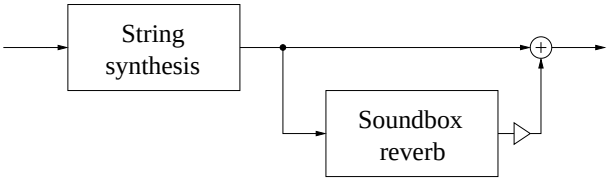

Figure 9: Simplified clavichord synthesis model incorporating a reverberation module to simulate the soundbox.

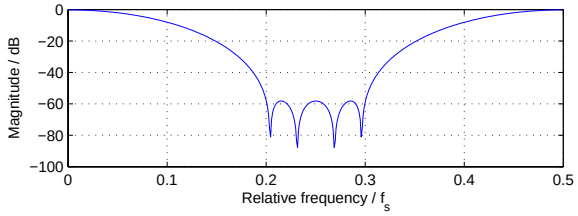

Figure 10: Frequency response of the input filter of the hypermeshes used in the clavichord soundbox impulse response simulation.

5. CONCLUSIONS AND FUTURE WORK

The hyperdimensional digital waveguide mesh discussed in this paper is a four-dimensional variation of the DWG mesh technique. The main advantage of this structure is its ability to provide a much more dense and irregural modal structure at high frequencies compared to meshes of lower dimensionality. In addition, the hypermesh is able to provide highly decorrelated output signals. These facts encourage the utilization of the presented technique, for example in the creation of artificial reverberation as presented in our paper. The attenuation characteristics of the mesh can be controlled by similar boundary conditions as used with 2-D and 3-D meshes, thus enabling shaping of the resulting magnitude response.

This paper has shown three different applications: a multi-channel reverberator, simulation of a lecture hall, and simulation of a clavichord soundbox. The quality obtained in these simple examples encourages to study further the uses

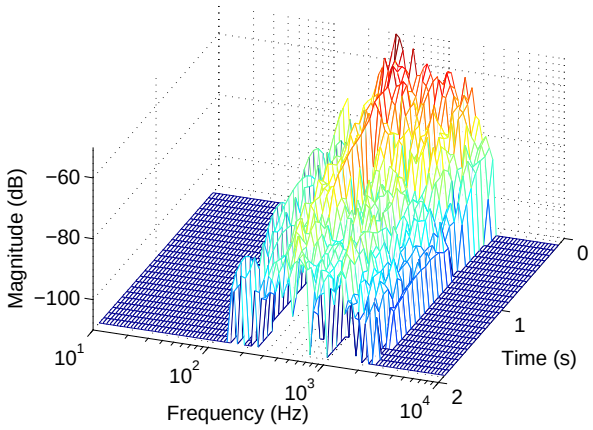

Figure 11: Combined response of the two hypermeshes used in the simulation of the clavichord soundbox impulse response. The low-frequency modes implemented with separate resonators are not included.

of hyperdimensional meshes in the field of spatial audio. All the examples and comparisons were performed with simple rectangular rooms. For more realistic simulations, more irregularly shaped spaces should be investigated, and the comparison should be extended to cover other reverberation techniques, such as the feedback delay networks, as well. In the future, listening tests should be performed to assess the sound quality.

REFERENCES

[1] S. A. Van Duyne and J. O. Smith III, "Physical modeling with the 2-D digital waveguide mesh," in *Proc. Int. Computer Music Conf.*, Tokyo, Japan, Sept. 1993, pp. 40–47.

[2] S. A. Van Duyne and J. O. Smith III, "The 2-D digital waveguide mesh," in *Proc. IEEE WASPAA*, New Paltz, NY, USA, Oct. 1993, pp. 17–20.

[3] J. O. Smith and G. P. Scavone, "The one-filter Keefe clarinet tonehole," in *Proc. IEEE Workshop on Applications of Signal Processing to Audio and Acoustics*, New Paltz, NY, October 1997.

[4] M. Karjalainen, V. Välimäki, and T. Tolonen, "Plucked-string models: from the Karplus-Strong algorithm to digital waveguides and beyond," *Computer Music Journal*, vol. 22, no. 3, pp. 17-32, Fall 1998.

[5] J. Bensa, S. Bilbao, R. Kronland-Martinet, and J. O. Smith, "The simulation of piano string vibration: from physical models to finite difference schemes and digital waveguides," *J. Acoust. Soc. Am.*, vol. 114, no. 2, pp. 1095-1107, 2003.

[6] F. Fontana and D. Rocchesso, "Physical modeling of membranes for percussion instruments," *Acustica united with acta acustica*, vol. 84, pp. 529–542, 1998.

[7] J. Laird, P. Masri, and C. N. Canagarajah, "Efficient and accurate synthesis of circular membranes using digital waveguides," in *Proc. IEE Colloquium on Audio and Music Technology: The Challenge of Creative DSP*, November 1998, pp. 12/1-12/6.

[8] L. Savioja and V. Välimäki, "Reducing the dispersion error in the digital waveguide mesh using interpolation and frequency-warping techniques," *IEEE Trans. Speech and Audio Processing*, vol. 8, no. 2, pp. 184–194, Mar. 2000.

[9] M. L. Aird, L. Laird, and J. ffitch, "Modelling a drum by interfacing 2-D and 3-D waveguide meshes," in *Proc. Int. Computer Music Conf.*, Berlin, Germany, Aug. 2000, pp. 82–85.

[10] S. Bilbao, "Sound synthesis for nonlinear plates," in *Proc. Int. Conf. Digital Audio Effects (DAFx)*, Madrid, Spain, September 2005, pp. 243-248, http://dafx05.ssr.upm.es/Proc_DAFx05/P_243.pdf.

[11] L. Savioja, T. Rinne, and T. Takala, "Simulation of room acoustics with a 3-D finite difference mesh," in *Proc. ICMC'94*, Aarhus, Denmark, Sept. 1994, pp. 463–466.

[12] L. Savioja, J. Backman, A. Järvinen, and T. Takala, "Waveguide mesh method for low-frequency simulation of room acoustics," in *Proc. 15th Int. Congr. Acoust. (ICA)*, Trondheim, Norway, June 1995, vol. 2, pp. 637-640.

[13] L. Savioja, J. Huopaniemi, T. Lokki, and R. Väänänen, "Creating interactive virtual acoustic environments," *J. Audio Eng. Soc.*, vol. 47, no. 9, pp. 675–705, Sept. 1999.

[14] P. Huang, S. Serafin, and J. O. Smith, "A 3-D waveguide mesh model of high-frequency violin body resonances," in *Proc. Int. Computer Music Conf.*, Berlin, Germany, Aug. 2000, pp. 86–89.

[15] M. J. Beeson and D. T. Murphy, "Virtual room modelling using hybrid digital waveguide mesh techniques," in *Proc. 147th meeting of ASA*, New York, USA, May 2004.

[16] G. R. Campos and D. M. Howard, "On the computational efficiency of different waveguide mesh topologies for room acoustic simulation," *IEEE Trans. Speech and Audio Processing*, vol. 13, no. 5, pp. 1063–1072, Sept. 2005.

[17] D. T. Murphy and D. M. Howard, "Modelling and directionally encoding the acoustics of a room," *Electronics Letters*, vol. 34, no. 9, pp. 864–865, Apr. 1998.

[18] A. Kelloniemi, V. Välimäki, and L. Savioja, "Simulation of room acoustics using 2-D digital waveguide meshes," *Proc. IEEE Int. Conf. Acoustics, Speech, and Signal Processing*, Toulouse, France, May 2006, vol. 5, pp. 313–316.

[19] J. Mullen, D. M. Howard, and D. T. Murphy, "Waveguide physical modeling of vocal tract acoustics: Flexible formant bandwidth control from increased model dimensionality," *IEEE Trans. Audio, Speech, and Language Processing*, vol. 14, no. 3, pp. 964–971, May 2006.

[20] D. Rocchesso and J. O. Smith, "Circulant andelliptic feedback delay networks for artificial reverberation," *IEEE Trans. Speech and Audio Processing*, 5(1), Jan. 1997, pp. 51–63.

[21] A. D. Pierce, *Acoustics, 2nd ed.* McGraw-Hill, New York, 1989, pp. 293–294.

[22] H. Kuttruff, *Room Acoustics, 4th ed.* Spon Press, London, 2000.

[23] V. Välimäki, J. Pakarinen, C. Erkut, and M. Karjalainen, "Discrete-time modelling of musical instruments," *Reports on Progress in Physics*, vol. 69, no. 1, pp. 1-78, January 2006, http://www.iop.org/EJ/abstract/0034- 4885/69/1/R01/.

[24] M. Karjalainen and C. Erkut, "Digital waveguides vs. finite difference schemes: Equivalence and mixed modeling," *EURASIP J. Applied Signal Process.*, no. 7, pp. 978–989, June 2004.

[25] F. Fontana, D. Rocchesso, "Signal-theoretic characterization of waveguide mesh geometries for models of two-dimensional wave propagation in elastic media," *IEEE Trans. Speech and Audio Process.*, vol. 9, no. 2, pp. 152–161, Feb. 2001.

[26] A. Kelloniemi, V. Välimäki, P. Huang, and L. Savioja, "Artificial reverberation using a hyper-dimensional FDTD mesh," in *Proc. European Signal Processing Conference (EUSIPCO)*, Antalya, Turkey, September 2005, http://signal.ee.bilkent.edu.tr/defevent/papers/cr1422.pdf.

[27] M. Karjalainen and H. Järveläinen, "More about this reverberation science: Perceptually good latereverberation," *AES 111th Convention*, New York, NY, USA, Nov. 2001, preprint no. 5415.

[28] A. Kelloniemi, "Frequency-dependent boundary condition for the 3-D digital waveguide mesh," *Int. Conf. Digital Audio Effects (DAFx)*, Montreal, Canada, Sept. 2006.

[29] H. Penttinen, M. Karjalainen, T. Paatero, and H. Järveläinen, "New techniques to model reverberant instrumentbody responses," in *Proc. ICMC'01*, Havana, Cuba, Sept. 2001, pp. 182–185.

[30] J.-M. Jot, "An analysis/synthesis approach to real-time artificial reverberation," in *Proc. ICASSP 1992*, San Francisco, California, U.S.A., Mar. 1992, vol. 2, pp. 221–224.

[31] J. O. Smith III, "Physical audio signal processing: for virtual musical instruments and digital audioeffects," online book at http://ccrma.stanford.edu/˜jos/pasp/, Center for Computer Research in Music and Acoustics (CCRMA), Stanford University.

[32] J. O. Smith III, "Efficient synthesis of stringed musical instruments," in *Proc. ICMC'93*, Tokyo, Japan, Sept. 1993, pp. 64–71.

[33] M. Karjalainen and V. Välimäki, "Model-based analysis/synthesis of the acoustic guitar," in *Proc. Stockholm Music Acoustics Conf.*, Stockholm, Sweden, Jul.-Aug., 1993, pp. 443–447.

[34] V. Välimäki, M. Laurson, and C. Erkut, "Commuted Waveguide Synthesis of the Clavichord," *Computer Music J.*, 27(1), pp. 71–82, Spr. 2003.

[35] V. Välimäki, H. Penttinen, J. Knif, M. Laurson, and C. Erkut, "Sound synthesis of the harpsichord using a computationally efficient physical model," EURASIP J. on Applied Signal Processing, no. 7, pp. 934–948, June 2004. Special Issue on Model-Based Sound Synthesis.